INTERNATIONAL ATOMIC ENERGY AGENCY
UNITED NATIONS EDUCATIONAL, SCIENTIFIC AND CULTURAL ORGANIZATION
INTERNATIONAL CENTRE FOR THEORETICAL PHYSICS
I.C.T.P., P.O. BOX 586, 34100 TRIESTE, ITALY, CABLE: CENTRATOM TRIESTE

H4.SMR/638-7

College on Medical Physics: Imaging and Radiation Protection

31 August - 18 September 1992

Dosimetric Methods and Techniques

S. Mascarenhas

NPDIA - EMBRAPA and Inst. Phys. and Chem.
Universidade de Sao Paulo
Sao Carlos, SP
Brazil

COLLEGE ON MEDICAL PHYSICS

IMAGING AND RADIATION PROTECTION

31 August - 18 September 1992

DOSIMETRIC METHODS AND TECHNIQUES

SERGIO MASCARENHAS

NPDIA - EMBRAPA and INST. PHYS. and CHEM.
UNIV. SAO PAULO, SAO CARLOS, SP.
BRAZIL

COLLEGE ON MEDICAL PHYSICS-ICTP-1992

DOSIMETRIC METHODS AND TECHNIQUES

PROF SERGIO MASCARENHAS

INTRODUCTION

In previous lectures during this College the various concepts of radiation fields were considered. In this short introduction we want to remind you of the main Dosimetric Units in use for the measurement of radiation. We shall be mainly concerned with photons from gamma and X-rays sources.

EXPOSURE - X - is the quotient of dQ by dm where dQ is the total electrical charge produced by radiation in a mass dm of air.

$$X = dQ/dm$$

The UNIT of EXPOSURE was previously called the ROENTGEN, symbol R, but the present international accepted Unit is the C/kg (coulomb per kilogram). This way :

$$1R = 2.58 \times 10^{-4} \text{ C/kg}$$

ABSORBED DOSE - symbol D

When radiation passess through matter it looses energy, or transfers energy to matter and the various aspects of radiation interaction with matter have also been previously studied in this College and we will assume it to be known. A very important concept arising from energy transfer to matter is that of ABSORBED DOSE, D which is quantitatively measured by the quotient of dE , the mean energy imparted to matter, and the mass dm

$$D = dE/dm$$

The unit of Absorbed Dose was previously called the RAD but the present accepted international Unit is now the GRAY, equivalent to the absorption of one joule (J) per quilogram (kg). The relation between the rad and the gray (Gy) is

$$1\ Gy = 100\ rads$$

QUALITY FACTOR- symbol Q, is a quantity obtained experimentally that measures the biological effect of radiation due to the absorbed dose D. This of course may change with the type of radiation and the organ or tissue considered.

DOSE EQUIVALENT - symbol H, is obtained from the Absorbed Dose D multiplied by the QUALITY FACTOR Q

$$H = QxD$$

also given in C/kg and the Unit is called SIEVERT (Sv).

The previous magnitude for dose equivalent was the REM and for the same type of radiation and tissue or organ

$$1\ rem = 100\ Sv$$

For radiation protection it is important to establish a MAXIMUM PERMISSIBLE DOSE EQUIVALENT, MPDE, of course for the various situations occurring, such as with radiation workers or the population in general. These limits for MPDE are the subject of constant analysis and discussion by International Agencies or Commissions, and will be focused in other lectures during this College.

TABLE I is a summary of the various quantities and unities just discussed.

TABLE I

MAGNITUDE	NEW UNIT	OLD UNIT	RELATION
EXPOSURE	C/kg	Roentgen	2.58×10^{-4}
ABS.DOSE	J/kg(Gy)	Rad	100
DOSE EQUIV.	J/kg(Sv)	Rem	100

How to measure and/or calculate these magnitudes is the object of RADIATION DOSIMETRY, and a discussion of some selected methods and techniques is the object of our lectures in this College.

DOSIMETRIC METHODS AND TECHNIQUES

We may generally classify dosimetric methods according to the main phenomena involved. The general idea is that radiation impinging on a material (gas, solid or liquid) will change its physical or chemical properties and the quantitative measurement of such changes will provide a DOSIMETRIC METHOD and corresponding DOSIMETRIC TECHNIQUE.

A reasonable classification(though not the only or best) is the following(see TABLE II)

TABLE II

METHOD	TECHNIQUE
IONIZATION METHODS	ION CHAMBER DOSIMETRY
	SEMI-CONDUCTOR JUNCTION
	ELECTRET DOSIMETRY
THERMAL METHODS	THERMOLUMINESCENCE DOSIM.
	CALORIMETRIC DOSIMETRY
	THERM.STIMUL.CONDUC.DOS.
	PYRO AND PIEZO ELECT.D
	THERMOPHOTOACOUSTIC DOS.
OPTICAL METHODS	FILM DOSIMETRY
	COLOUR CENTER DOSIMETRY
	LYOLUMINESC. DOSIMETRY
MAGNETIC METHODS	ELECTRON SPIN RES. DOSIM.
CHEMICAL METHODS	FRICKE OPT.ABS.DOSIMETRY
	REDOX REACTIONS DOSIMETRY
	ETCHING TECHNIQUES DOSIM.

In the following lectures with the cooperation of Profs. H. Farach and O. Baffa (for ESR), P.Cruvinel (electrets) and A.A.Carvalho (pyro,piezo and thermoacoustical dosimetry), we will be discussing the general principles or in some cases experimental details and research possibilities of these methods some of which have been introduced by our research group in Brazil.

THERMOLUMINESCENCE DOSIMETRY(TLD)

One of the most important and useful method of dosimetry is TLD. This was introduced as materials science progressed and the controlled growth and preparation of crystals was achieved.

The main idea behind the method is the following: When a dielectric or semiconductor is irradiated ,carriers such as electrons and holes are produced . One has to bear in mind that band gaps between valence and conduction bands are of the order of a few eV. Photons or particles having much larger energies than this (keV) will excite electrons from the valence band to the conduction band and this may be experimentally detected by measuring the electric current during irradiation with an applied electric field. Of course the real situation is not that simple,the material usually contains defects and impurities and these may also be excited and/or capture electrons and holes (recombination). Once irradiation, at a certain temperature T is stoped we will be left with a sample containing a certain number n(0) of filled traps. This is just the first part of the process. Now we proceed to heat the sample, at a certain heating rate b

$$b = \frac{dT}{dt} \qquad (1)$$

where t is the time. During this heating some (or all) of the charges (electrons or holes) will be evaporated from traps and may recombine with other carriers in the valence band or even in other recombination centers . This recombination may occur in several ways, but it may lead to radiative(emmision of light,luminescence) and/or non- radiative transit(loosing energy to lattice vibrations,phonons,that is heat).

All these processes may be represented by fig 1 a simplified configuration coordinates diagram and band model for TLD emmission.

We may now introduce a simple quantitative model for TL emmission which will serve as a basis for TL dosimetry (TLD).

During heating, at a constant rate b, recombination may

lead to so-called GLOW CURVES if ones plot intensity I of light emmission as a function of temperature T . Fig 2 ilustrates a typical glow curve for one of the most important materials which are able to luminesce(and thus called a PHOSPHOR), namely LiF.

Pure LiF will not always luminesce after irradiation, the material has do be purified,doped and thermally treated to present adequate behaviour for dosimetry. The finding of proper conditions for the phosphor is an important part of the research done in TLD . For instance , Prof. J.R. CAMERON, pioneered TLD research and was one of the main scientists to introduce LiF with proper doping(Mg+Ti and other combinations). This was then given general and universal importance by being consistently and reliably produced in many labs(academic and industrial). Today one can order LiF pellets, of small size(a few mm square) or powder to be used in several situations in radiation dosimetry.

As one can see from the GC(glow curve) several peaks may be present. In this case the phosphor may have several traps at different trapping levels E(n). Of course deep levels will evaporate at higher temperatures T(n). This is because release of the carrier from the trap will follow an exponential function,

$$p = f.e^{-\frac{E(n)}{kT}} \qquad (2)$$

where p is the probability of release, f is a frequency factor(roughly the number of times per second the carrier tries to jump the energy barrier),k the Boltzman constant and T the absolute temperature.

The rate at which carriers will be released may be written as

$$\frac{dn}{dt} = n.f.e^{-\frac{E(n)}{kT}} \qquad (3)$$

assuming n to be the carrier density (number of carriers per cm3), at the traping level at time t and temperature T.

Now more simplifying assumptions are introduced to get a

corresponding simple model: we assume that once the carriers are detraped they do not recombine again during heating, and most important that the TL intensity (I), will be proportional to the rate of release :

$$I = -C.\frac{dn}{dt} \qquad (4) \qquad (4)$$

where C is a constant. If the rate of heating is constant starting with n_0 carriers from an initial T(i) to a maximum temperature T(m) and integrating, we get

$$I = n_0.C.f.e^{-\frac{E(1)}{kT(M)}}.e^{-\int_{T_i}^{T_f}\frac{f}{b}.e^{-\frac{E(1)}{kT}}.dT} \qquad (5)$$

The magnitude of the integral of I corresponds to the area under the glow curve between the temperature of irradiation T_i and the maximum temperature T_f. Of course the peak will occur at the maximum peak temperature T(M). Care must be taken to subtract the black-body emmision of the phosphor and other back-ground light. In the experimental situation this is easily done by re-heating the phosphor again.

Another way to measure the total intensity is by using I(M) the intensity at the maximum and assume that the half-width of the peak is approximately constant. Of course the total intensity is proportional to n(0) which is the dosimetric quantity. What one does in practice is to obtain a calibration curve of integrated intensity(area under the peak) or peak intensity I(M) as a function of dose of irradiation D. For a "good" phosphor this should be preferably linear. For the case of LiF-100(Harshaw type) this linearity may hold up to 6 Gy for the usual range of energies used in radiology and radiotherapy.

The energy dependence of the phosphor, relative response normalized to Co radiation for instance, is also a very important parameter. Of course this will depend on the type of material of the phosphor . One would like to have a dependence similar to soft tissue for personal radiation protection . For LiF the

energy dependence is given in fig 2.

EXPERIMENTAL ASPECTS OF TLD

In order to measure TL and the corresponding glow curves one uses the following experimental set-up (fig 3).
The emmited radiation (light whose spectrum can also be investigated), is measured with a photomultiplier PM, choosen to be sensitive to the wave-lenght of the emmited light,in the blue for LiF for example. The output from the photomultiplier goes to a sensitive electrometer E. The output of this electrometer is either integrated or goes to a peak detector D. It may be useful to use a pen recorder PR to observe the glow curves (ploting current and temperature in the XY recorder. The heating is obtained in several ways: by direct electrical heating of the planchette P where the phosphor sits, by laser light, by a heating gas etc. Filters F may be used to block infrared or select bands in the emmission spectrum.

Of course nowadays the equipment may be interfaced to a computer, feeding of the phosphor(usually in the form of pellets or pre assembled badges) may also be automated and a dedicated software is used for corrections, changing and controlling rates of heating, identification of the badges ,storing and processing of data in required formats. During this College we will have practical sessions with different commercial equipments. We have however built our own TLD reader in S.Carlos,Brazil,including the electrometer,heater etc which has been in continuos use now for more than 10 years with no problems. A final experimental observation must be made: usually one must use dry-nitrogen gas over the sample to avoid spurious luminescence(probably from Oxygen and other surface effects). The pressure of the gas must be controlled for it affects the loss of heat and thus the heating rate. The heating rate changes the glow-curve as can be seen from the equations. Usually one tries to keep heating rates

constants of the order of a few degrees per second. Slow heating may lead to overlapping peaks, too high to non-linearities in calibration curves and other undesirable effects.

In practice the following points are of great importance:

-The phosphor should be thermally treated and calibrated before use . This implies heating the phosphors in an oven according to the protocol recommended for that kind of phosphor. The reason for this is to clean trapping centers, erase memory-effects due to preparation of phosphor such as attaining proper annealing of the samples . Of course time of heating, cooling of the phosphors , proper cleaning of the surfaces are details to be observed. Modern TLD readers have automated cycles for thermal treatment of phosphors.

-Calibration curves of reading versus dose should be obtained in the dose range desired and with appropriate irradiation conditions(badges,filters,types of radiation energies etc). For precision dosimetric work phosphors may have to be grouped and even calibrated individually.

-Calibration of optical ,thermal and electrical responses of the reader should be permanently checked.

-Phosphors present isothermal decay(fading) and can also fade under light,mechanical or chemical treatment.They also change their calibration after repeated use and have a maximum integrated dose to be observed.

Prof.J.R. Cameron besides being one of the pioneers of TLD has implanted in many Third World Countries TLD in place of film dosimetry and he is the foremost authority for consultation in this field. Since he will be present in this 1992 College only between the 3rd and 9th of Sept participants should have consultations and questions prepared for him. Of course we shall also have Drs. Padovani and Contento from Udine as specialists

for TLD Lab experiments who can and should be consulted. A short list of references is also given with these notes.

To close this discussion we would like to stress that TLD is very important for almost all fields of Medical Physics for which dosimetry is required such as personal and environment dosimetry, radiology, radiotherapy, nuclear medicine as well as it still is a field open for research in basic and applied aspects.

For instance in many Third World countries there are active groups doing research in TLD phosphors, crystal growth, natural ocurring crystals and materials, instrumentation for TLD and many other aspects. It is thus an area of importance for Medical Physics in the Third World, in particular because it does not require expensive equipment and has ,as said above, basic (experimentally and theoretically) and applied aspects.

Nuclear Instruments and Methods in Physics Research A287 (1990) 580–582
North-Holland

A PORTABLE ELECTRONIC SYSTEM FOR RADIATION DOSIMETRY USING ELECTRETS

P.E. CRUVINEL [1], S. MASCARENHAS [1] and J. CAMERON [2]

[1] *EMBRAPA/UAPDIA, P.O. Box 741, S. Carlos, SP, 13560, Brazil*
[2] *University of Wisconsin, Madison, WI 53706, USA*

Received 30 March 1989 and in revised form 12 September 1989

An electret dosimeter with a cylindrical active volume has been introduced by Mascarenhas and collaborators [Proc. 10th Anniversary Conf. 1969–1979, Associação Brasileira de Fisicos em Medicina, p. 488; Topics Appl. Phys. 33 (1987) 321] for possible use in personnel and area monitoring. The full energy response curve as well as the degree of reproducibility and accuracy of the dosimeter are reported in a previous report [O. Guerrini, Master Science Thesis, São Carlos, USP-IFQSC (1982)].

For dimensions similar to those of the common pen dosimeter, the electret has a total surface charge of the order of 10^{-9} C and it has a readout sensitivity of the order of 10^{-5} Gy with a useful range of 5×10^{-2} Gy.

In this paper we describe a portable electronic system to measure X and γ-rays using a cylindrical electret ionization chamber. It uses commercially available operational amplifiers, and charge measurements can also be made by connecting a suitable capacitor in the feedback loop.

With this system it is possible to measure equivalent surface charges up to (19.99 ± 0.01) on the dosimeter. The readout doses are shown on a $3\frac{1}{2}$ digit liquid crystal display (LCD). We have used complementary metal oxide semiconductor (CMOS) and bipolar metal oxide semiconductor (BiMOS) operatonal amplifier devices in the system's design. This choice provides small power consumption and is ideal for battery powered instruments.

Furthermore the instrument is ideally suited for in situ measurements of X and γ radiation using a cylindrical electret ionization chamber.

1. System's design

The block diagram and electronic circuit of the apparatus are shown in figs. 1 and 2 respectively. This arrangement allows measurements to be made of dosimeter performance and characteristics, such as decay leakage, and may be used in hospitals, research laboratories as well as in nuclear centers. The equivalent surface charge on the electret of the dosimeter may be read directly into a $3\frac{1}{2}$ LCD display.

1) Cylindrical readout electrode. The cylindrical readout electrode is attached to the electrometer. The charge or voltage induced on the readout electrode is proportional to the uncompensated charge on the electret.

2) Electrometer. This subsystem is used to measure the equivalent surface charge on the electret. This measurement provides the quantitative evaluation of the radiation dose to which the dosimeter has been exposed. The integration preamplifier consist of a commercially available operational amplifier (opamp) No. CA3140A and uses a capacitor in the feedback loop. The CA3140A BiMOS operational amplifiers feature gate-protected MOS/FET (PMOS) transistors in the input circuit to provide very-high-input impedance, very-low-input current, and high-speed performance.

3) A/D converter. This subsystem is used to convert the analog signal from the electrometer to a digital signal for readout in a $3\frac{1}{2}$ LCD display. We have been using a ICL7106 as the A/D converter.

4) Latch control. This subsystem enables or disables the digital data transfer from the A/D converter to the LCD display. In this way we have a relationship between the cylindrical readout electrode and the integration time. Thus data can be latched on the LCD display.

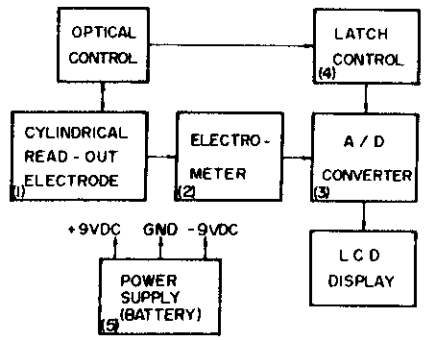

Fig. 1. Block diagram of the portable electronic system for radiation dosimetry using electrets.

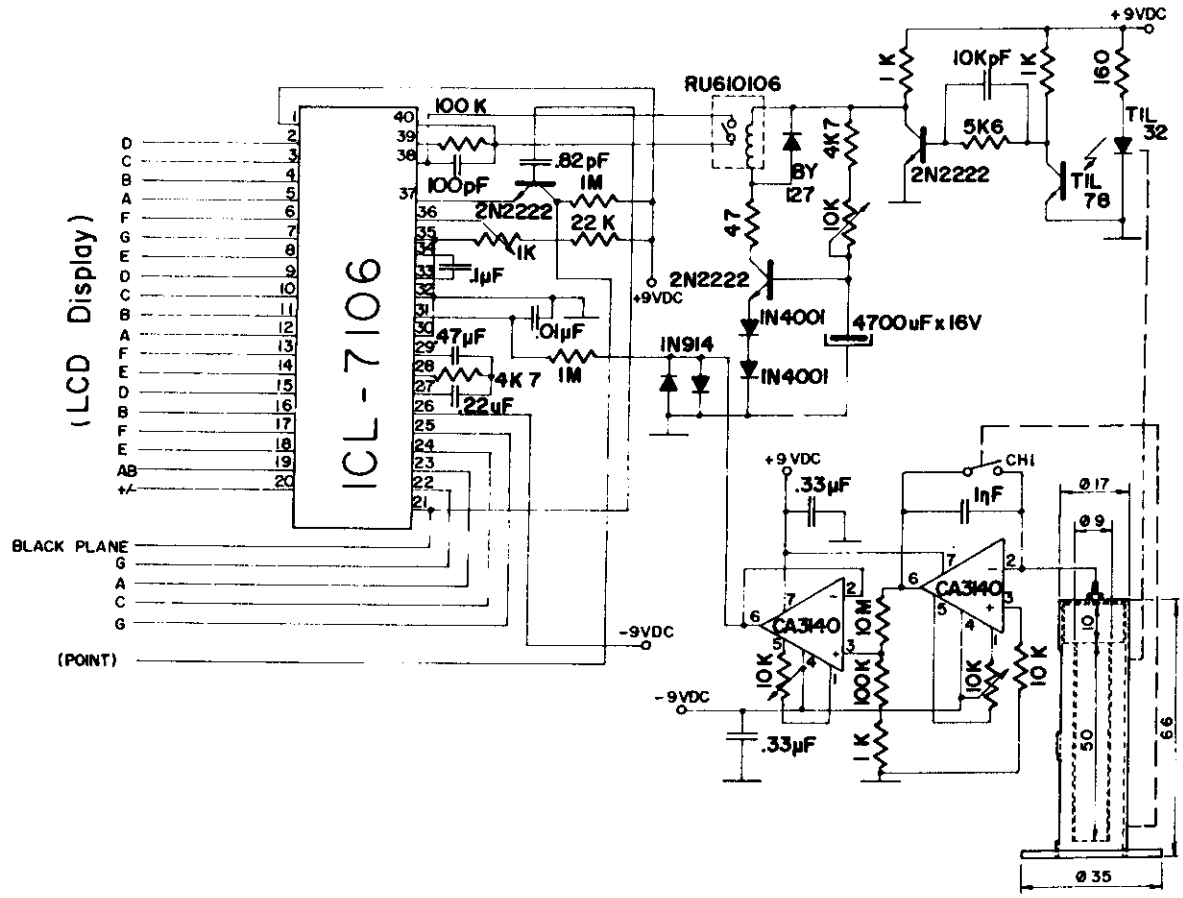

Fig. 2. Electronic circuit of the apparatus (resistors in Ω).

5) Optical control. This subsystem identifies whether the dosimeter is or not inside the cylindrical readout electrode. We have used a P–N gallium arsenide infrared-emitting diode (TIL 32) and a N–P–N silicon phototransistor (TIL 78).

2. Experimental procedure and discussion

The use of electrets for dosimetry has recently been reviewed by Gross [1]. Recent contributions in which electric fields for an ionization chamber are produced by an electret have been reported by Bauser and Runge [2] and Ikeya [3]. The stability of liquid charged electrets has been reported by Chudleiger, Collins and Hancock [4]. We used for our experiments cylindrical electret ionization chambers as reported by Cameron and Mascarenhas [5]. In these ionization chambers, the electret also serves as the detector by measurement of the remaining uncompensated charge after exposure to ionizing radiation.

The surface of teflon FEP® electrets film was charged by the Corona discharge method.

The electrets were charged negatively and typically induced an electric field of > 1000 V/m in the enclosed air gap of the ionization chamber.

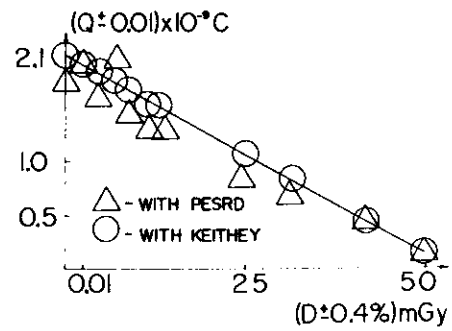

Fig. 3. Experimental results for (10 mA, 60 kV) X-rays ($Q = -0.039D + 2.09$; $r^2 = 0.98$).

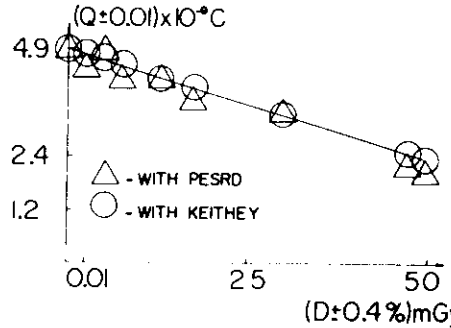

Fig. 4. Experimental results for (^{60}Co) γ-rays ($Q = -0.05D + 4.89$; $r^2 = 0.97$).

A total surface charge of the order of 10^{-9} C and a readout sensitivity of the order of 10^{-5} Gy with a useful range up to 5×10^{-2} Gy were reached. The readout method involves removing a cap from the ionization cylindrical readout electrode which is attached to the electrometer circuit. The charge or voltage induced on the readout electrode is proportional to the uncompensated charge on the electret.

Experimental results with the dosimeters are reported in figs. 3 and 4. These results were obtained with (10 mA, 60 kV) X-ray and (^{60}Co) γ-ray exposure respectively, by using a portable electronic system for radiation dosimetry (PESRD) and a regular Keithley 616 digital electrometer for readout comparison.

Fig. 5 shows a photograph of the model and gives several characteristics.

3. Conclusions

The main features of this system are:

i) Easy adjustment and calibration.

ii) Low power dissipation and zero drift (less than 2 μV/° C).

iii) The measurement stage of the equivalent surface charge of the electret has offset compensation and automatical reset of the active integrator.

iv) The experimental results show the possibility of using the PESRD in radiation dosimetry and particularly in personnel and area monitornig dosimetry.

v) The system is useful for studies of charge stability [6] of electret dosimeters.

vi) The system may be used in hospitals, research laboratories as well as in nuclear centers for dosimetry.

Acknowledgements

The authors gratefully acknowledge CNEN, FINEP, CNPq and EMBRAPA/UAPDIA for the financial and institutional support.

References

[1] B. Gross, Topics Appl. Phys. 33 (1980) 217.
[2] H. Bauser and W. Runge, Health Phys. 34 (1978) 97.
[3] M. Ikeya and T. Miki, Technical College, Yamaguchi, Univ. Ube 755, Japan, private communication.
[4] P.W. Chudleigh, R.E. Collins and G.D. Hancock, Appl. Phys. Lett. 23 (1973) 211.
[5] J. Cameron and S. Mascarenhas, Nucl. Instr. and Meth. 175 (1980) 117.
[6] J. Van Turnhout, Topics Appl. Phys. 33 (1987) 81.

Fig. 5. Photograph of the model. Dimensions and weight: (w × h × d): 125 × 70 × 135 mm; weight: 0.48 kg.

PIEZO AND PYROELECTRIC RADIATION DOSIMETRY

Aparecido Augusto de CARVALHO
Departamento de Engenharia Elétrica, UNESP, C.P. 31, 15378, Ilha Solteira, SP, Brazil

and

Sergio MASCARENHAS
EMBRAPA/NPDIA, C.P. 741, and IFQSC/USP, C.P. 369, 13560, São Carlos, SP, Brazil

Abstract

In this paper we review the use of photoacoustic and pyroelectric radiation dosimeters. We compare the characteristics and results obtained with a photoacoustic radiation dosimeter (PARD) and a pyroelectric radiation dosimeter (PERD). The PARD and the PERD can be used to measure the energy fluence rate of continuous x-ray beams. In the same way, the single-pulse photoacoustic radiation dosimeter (PPARD) and the single-pulse pyroelectric radiation dosimeter (PPERD) were compared. They can measure the energy fluence of a single pulse of x-radiation. A theoretical model to explain the results obtained with the PPERD is presented and compared with experimental results.

1. Introduction

We have proposed new methods to measure x-radiation energy fluence rate using photoacoustic and pyroelectric dosimeters since 1984. S. Mascarenhas et al. reported the use of the photoacoustic radiation dosimeter (PARD) for x-rays and described its main characteristics [1]. M.H. de Paula et al. described the pyroelectric radiation dosimeter (PERD) also in 1984 [2]. Both have used to measure the radiation fluence rate of continuous x-ray beams in the diagnostic range.

Recently, A.A. Carvalho et al. proposed two thermal methods to measure the energy fluence of a brief exposure of diagnostic x-rays [3]. The single-pulse photoacoustic radiation dosimeter (PPARD) and the single-pulse pyroelectric radiation dosimeter (PPERD) produces an electrical signal wich is proportional to the energy fluence of the x-ray beam.

Conventional photoacoustic techniques involve the detection of thermal or acoustic waves generated by the absorption of eletromagnetic radiation in a sample. The sample, in an enclosed gas filled cell, is excited with a modulated radiation beam producing periodic heating of the sample. This causes mechanical deformation of the sample as well as a temperature variation in the sample and in a thin layer of the gas at the gas-sample boundary. The resulting pressure variation at the chopped frequency is usually converted to an electrical signal by a sensitive microphone in the cell [4]. In PARD and PPARD the sample is a Pb disk which absorbs about 99.9% of the x-ray energy used in these studies.

In pyroelectric materials its spontaneous polarization

is strongly temperature dependent. The pyroelectric coefficient p is defined as the partial derivative of the polarization with respect to the temperature. The pyroelectric effect may be used as a sensitive bolometer, capable of measuring power levels as low as 10^{-10} W [5]. A pyroelectric detector is usually a thin wafer of a pyroelectric material oriented with the electrode surfaces normal to its polarization vector. When radiation power is absorbed by the detector its temperature changes. The change in detector temperature alters its polarization and causes a change in the surface charge through the pyroelectric effect. The change in the surface charge produces an electrical output signal that is proportional to the incident radiation power. The pyroelectric detector responds to the rate of change of temperature. Thus it can only be used to measure modulated or pulsed radiation power. In PERD and PPERD we used as detector a lead zirconium titanate (PZT) material. The detector characteristics were not effected by radiation absorbed. Its output remained practically unchanged for doses up to 3×10^7 Gy of x-rays in the diagnostic range.

2. Materials and Methods

The x-ray source, model MG 150, Muller, was a full wave rectified, single-phase unity. It could be operated in the range between 50 kVp and 90 kVp with currents up 20 mA. The total filtration in the beam was 2 mm Al.

All measurements were made using the same geometry. The distance from the target to the pyroelectric detector or the

photoacoustic cell window was 7 cm. The irradiated area of the detectors was 44 mm^2. Exposure measurements for conditions similar to those used for these studies had a standard deviation of 5 percent. The exposure was measured with low-energy ion chambers (Model 651, Victoreen) placed at the same position of the detectors.

The PARD consists basically of a photoacoustic cell, a x-ray beam chopper to modulate the incident radiation and a lock-in amplifier to measure the photoacoustic signal by synchronous detection. This is shown schematically in Fig. 1.

We used a nonresonant photoacoustic cell built in our own laboratory with an electret microphone with a sensitivity of 5.3 mV/Pa. The sample in the photoacoustic cell was a Pb disk 10 mm diameter and 0.6 mm thick. A duct 1 mm in diameter led from the sample chamber to the microphone chamber. The cell windows was lucite 1 mm thick.

The components of the PERD were essentially the same as the PARD with the photoacoustic cell replaced by a pyroelectric chamber. The pyroelectric chamber, seen in Fig. 2, consists basically of a lead zirconium titanate (PZT) material (17 x 17 mm and 3 mm thick, from Edo. Western Corporation, Salt Lake City, UT) on a nylon support inside a chamber which was capable of being evacuated to about 100 Pa. A thin (25 μm) Mylar allows the entrance of the x-ray beam. The detector absorbs more than 99.7% of the x-ray beam energies used in these studies (50-90 kVp).

To measure the energy fluence of a brief x-ray exposure we developed PPARD and PPERD. The componentes of PPARD were an x-ray shutter, a photoacoustic cell and an electronic peak

detector.

The x-ray source used in these studies had no provision for short exposure so radiation pulses were obtained with a motor driven lead shutter (Fig. 3). The x-ray shutter was a Pb disk 3 mm thick with a 8.0 mm x 5.5 mm hole 8.5 cm from the axis, driven by a motor. An x-ray pulse was produced when the orifice of the x-ray shutter was aligned with the circular orifice of a collimation Pb plate and the Pb sample, inside the photoacoustic chamber. The exposure time was 0.26 s. An aspect of crucial importance in the design of the photoacoustic cell was to minimize the scattered radiation on the microphone because it generates large spurious signals. We measured the amplitude of the electrical pulse produced in the output microphone with a X-Y recorder (Model 7004 B, Hewlett Packard).

The componentes of PPERD are essentially the same of the PPARD with the photoacoustic cell replaced by the pyroelectric chamber. Fig. 4 shows the waveform of the electrical pulse produced by the PPERD. The pulse was slow (about 2 s) and could be recorded without distortion.

The instrument used for radiation calibration purposes was a thimble type ionization chamber that measured exposure. The energy fluence was calculated from the measured exposure and effective energy of the beam. The equivalent photon energy of the beam was determined by measuring the half-value layer [6].

3. Theoretical Model

The difference of temperature ΔT between the pyroelectric detector and its surroundings is related to the incoming radiation power P(t), receveid by the detector, by the equation:

$$H \, d \frac{\Delta T}{dt} + G_R \, \Delta T = \eta \, P(t) \tag{1}$$

where:

H = thermal capacitance of the detector

G_R = average thermal radiative conductance

η = emissivity of the surface

By solving the equation (1), results

$$\Delta T = k \, e^{-\frac{t}{\tau_T}} + e^{-\frac{t}{\tau_T}} \int_0^t e^{\frac{\theta}{\tau_T}} \frac{P(\theta)}{H} \, d\theta \tag{2}$$

with

k = a constant

$\tau_T = H/G_R$ = thermal time constant of the detector

Fig. 5 shows the equivalent electrical circuit of the detector and input preamplifier. The preamplifier used has two stages.

The expression for the signal V(t) in the output of the preamplifier first stage is:

$$C_1 \frac{dV(t)}{dt} + \frac{V(t)}{R_1} = i_d(t) \tag{3}$$

$$\therefore \quad \frac{dV(t)}{dt} + \frac{V(t)}{\tau_{E_1}} = \frac{A_d\, p}{C_1}\, d\, \frac{\Delta T}{dt} \tag{4}$$

where:

p = pyroelectric coefficient

A_d = detector area

$\tau_{E_1} = R_1 C_1$ = electrical time constant of pyroelectric detector and preamplifier first stage.

Solving Eq. 4 with the initial condition $V(t) = 0$ for $t = 0$, results [7]:

$$V(t) = \frac{A_d\, p}{HC_1}\left[\frac{\tau_T}{\tau_T - \tau_{E_1}}\, e^{-\frac{t}{\tau_{E_1}}} \int_0^t P(\theta) e^{\frac{\theta}{\tau_{E_1}}}\, d\theta - \frac{\tau_T}{\tau_T - \tau_{E_1}}\, e^{-\frac{t}{\tau_T}} \int_0^t P(\theta) e^{\frac{\theta}{\tau_T}}\, d\theta\right] \tag{5}$$

The Laplace transform of Eq. 5 is:

$$V(s) = \frac{A_d\, p}{HC_1}\, \frac{P(s)}{(s+\frac{1}{\tau_T})(s+\frac{1}{\tau_{E_1}})} \tag{6}$$

Fig. 6 shows the diagram of the preamplifier second stage.

The Laplace transform in the output of the preamplifier second stage is given by:

$$V_0(s) = \frac{A_d\, p.Z}{HC_1}\, \frac{s^2}{(s+\frac{1}{\tau_T})(s+\frac{1}{\tau_{E_1}})(s+\frac{1}{\tau_{E_2}})}\, .\, P(s) \tag{7}$$

where:

$Z = 1 + R_4/R_3$ (8a)

$\tau_{E_2} = R_2 C_2$ = electrical time constant of the preamplifier second stage (8b)

Fig. 7 shows the cross section of the collimated x-ray beam in a convenient coordinate system.

The intensity of the x-ray beam is uniform. Then $I(x,y) = I_0$ and $P = I_0 A_b$, where P is the power of the incident radiation, r is the radius of the x-ray beam, and $A_b = \pi r^2$ is the area of the cross section of the x-ray beam.

The window of the shutter deslocates uniformely with x and the power P varies with x, accordly Eq. 9.

$$P = I_0\left[r^2 \operatorname{sen}^{-1} \frac{\sqrt{r^2-x^2}}{r} - x\sqrt{r^2-x^2}\right] \qquad -r \leq x \leq 0 \tag{9a}$$

$$P = I_0\left[\pi r^2 - r^2 \operatorname{sen}^{-1} \frac{\sqrt{r^2-x^2}}{r} + x\sqrt{r^2-x^2}\right] \qquad 0 \leq x \leq r \tag{9b}$$

In our experiment, the window deslocated from -r to r in 0.13 s.

Fig. 8 shows the waveform of the power of the x radiation pulse that strikes the pyroelectric detector.

The inclusion of the power equations in the Eq. 7 becomes the solution of this equation matematically complex. Because this we approach the waveform seen in Fig. 8 by the waveform shown in Fig. 9.

The signal seen in Fig. 9 is a sum of four ramp signals as shown in Fig. 10.

$$P_1(t) = \frac{Pm}{0.13-z}\, t \qquad t \geq 0 \qquad (10a)$$

$$P_2(t) = 0 \qquad t < 0.13-z \qquad (10b)$$

$$P_2(t) = \frac{Pm}{0.13-z}\,[t-(0.13-z)] \qquad t \geq 0.13-z \qquad (10c)$$

$$P_3(t) = 0 \qquad t < 0.13+z \qquad (10d)$$

$$P_3(t) = \frac{-\,Pm}{0.13-z}\,[t-(0.13+z)] \qquad t \geq 0.13+z \qquad (10e)$$

$$P_4(t) = 0 \qquad t < 0.26 \qquad (10f)$$

$$P_4(t) = \frac{Pm}{0.13-z}\,(t-0.26) \qquad t \geq 0.26 \qquad (10g)$$

$$\text{If } P(t) = bt \rightarrow P(s) = b/s^2 \qquad (11)$$

Substituting the Eq. 11 in Eq. 7 and considering that the electrode that received the radiation was grounded, we obtain:

$$V_0(s) = -\frac{A_d \cdot p}{HC_1}\,\frac{b}{(s+\frac{1}{\tau_{E_1}})(s+\frac{1}{\tau_{E_2}})(s+\frac{1}{\tau_T})} = \frac{AA}{s+\frac{1}{\tau_{E_1}}} + \frac{BB}{s+\frac{1}{\tau_{E_2}}} + \frac{CC}{s+\frac{1}{\tau_T}} \qquad (12)$$

$$b = \frac{Pm}{0.13-z} = \frac{A_b \cdot \psi}{0.13-z} \qquad (13)$$

where ψ = energy fluence rate.

Solving Eq. 12 we obtain AA, BB and CC.

$$V_0(t) = AA\, e^{-\frac{1}{\tau_{E_1}}} + BB\, e^{-\frac{1}{\tau_{E_2}}} + CC\, e^{-\frac{t}{\tau_T}} \qquad (14)$$

Hence, the final expression for the signal in the output of the preamplifier second stage results:

$$V_0(t) = m\left[\tau_{E_1}(\tau_{E_2}-\tau_T)\, e^{-\frac{t}{\tau_{E_1}}} + \tau_{E_2}(\tau_T-\tau_{E_1})e^{-\frac{t}{\tau_{E_2}}} + \tau_T(\tau_{E_1}-\tau_{E_2})e^{-\frac{t}{\tau_T}}\right] \qquad (15)$$

where

$$m = \frac{A_d \cdot A_f\, p\, \tau_{E_1}\tau_{E_2}\tau_T\, \Psi}{HC_1(\tau_{E_2}-\tau_{E_1})(\tau_T-\tau_{E_1})(\tau_T-\tau_{E_2})} \qquad (16)$$

with Ψ = energy fluence

Finaly we obtain the signal $\bar{V}_0(t)$ int the output of the preamplifier in different time intervals, during and after the incidence of the pulse of x-rays in the detector.

$$\bar{V}_0(t) = V_0(t) \qquad 0 \leq t \leq 0.13-z \qquad (17a)$$

$$\bar{V}_0(t) = V_0(t)-V_0(t-0.13+z) \qquad 0.13-z\ t \leq 0.13+z \qquad (17b)$$

$$\bar{V}_0(t) = V_0(t)-V_0(t-0.13+z)-V_0(t-0.13-z) \qquad 0.13+z \leq t \leq 0.26 \qquad (17c)$$

$$\bar{V}_0(t) = V_0(t)-V_0(t-0.13+z)-V_0(t-0.13-z)+V_0(t-0,26) \qquad t \geq 0.26 \qquad (17d)$$

By using the equations above and the values of the parameters of the pyroelectric detector, preamplifier and radiation beam, we obtained the waveform of the electrical signal produced by PPERD for $\Psi = 0.83\ J/m^2$, using a microcomputer (Fig. 11).

Comparison with experiments

In the theoretical model presented the amplitude of the electrical signal is linear with the radiation energy fluence. This theory agrees with the experimental results obtained with the PPERD.

The waveform determined from the theoretical model approachs reasonably the experimental waveform. Thus we were able to explain the main features of the signal.

The differences between the experimental and the theoretical values are due the following factors:

1) In the model we considered the detector very thin so that we neglected any temperature gradient in the detector. In our radiation measurements we used a detector 3 mm thick and there is thermal diffusion through the material.

2) The values of the constants for the PZT were obtained in a table and are approximate values.

3) There is an uncertainty of approximately 10% in the computation of the radiation energy fluence due to innacuracy in the determination of the energy absorption coefficient of the air and the instability of the x-ray source.

4) We approached the real waveform of the power signal

of the beam by the waveform seen in Fig. 9.

4. Results

Fig. 12 shows the response of the PARD and PERD as a function of the x-radiation energy fluence rate at a chopping frequency of 13.8 Hz.

The noise signal of the PARD was 14 μV wich corresponds to the signal we would expect from an exposure rate of 0.48 R/s for 30 KeV radiation. The noise signal of PERD was 0.43 μV which corresponds to an exposure rate of 21.6 mR/S for 30 KeV radiation.

Fig. 13 illustrates the response of the PPARD and PPERD with the energy fluence.

The noise signal of the PPERD was about 0.1 mV which corresponds to the signal we would expect from 10 mR in a 0.26 s exposure of 30 KeV radiation. The noise signal of PPARD was 0.3 mV which corresponds to about 20 times that of the PPERD.

5. Conclusions

The PARD and PERD responds linearly to the radiation energy fluence rate. The PERD is more sensitive.

The PPARD and PPERD can measure the energy fluence from a single pulse of x-radiation incident on them. They can be used to determine the energy fluence associated with brief exposues such as used in diagnostic x-ray procedures. PPARD and PPERD are

simple, rugged and inexpensive instruments.

The results obtained with the PARD agree with the Rosencwaig-Gersho theory [8]. The Aamodt & Murphy theory explains the PPARD results [9]. The ideal pyroelectric detector theory justifies the results obtained with PERD [10].

The theoretical model that we proposed explains the results obtained with PPERD. In our model the amplitude of the electrical signal in linear with the radiation energy fluence rate. The waveform determined from the theoretical model approachs reasonably the experimental waveform and we were thus able to explain the main features of the signal.

Acknowledgements

We express our gratitude to Prof. J.R. Cameron, H. Vargas, M.H. de Paula, W.L.B. Melo and M.C.M. Teixeira. This work was supported by CAPES, CNPq, FINEP, FAPESP and CNEN in Brazil.

References

[1] S. Mascarenhas, H. Vargas and C.L. Cezar, "A photoacoustical radiation dosimeter", Med. Phys., Vol. 11, pp. 73-74, 1984.

[2] M.H. de Paula, A.A. de Carvalho, S. Mascarenhas and R.L. Zimmerman, "A new radiation dosimeter using a pyroelectric detector", Med. Phys., Vol. 11, pp. 866-868, 1984.

[3] A.A. Carvalho, S. Mascarenhas and M.H. de Paula, "Two thermal methods to measure the energy fluence of a brief exposure of diagnostic x-rays", Med. Phys., accepted for publication.

[4] F.A. McDonald, "The photoacoustic effect and the physics of waves", Am. J. Phys., Vol. 48, pp. 41-46, 1980.

[5] C.B. Roundy and R.L. Byer, "Sensitive $LiTaO_3$ pyroelectric detector", J. Appl. Phys., Vol. 44, pp. 929-931, 1973.

[6] H.E. Johns and J.R. Cunningham, "The Physics of Radiology", 4th edition, Thomas Springfield, 1983, Chapters 7 and 8.

[7] L.S. Kremenchugskii and R.Y. Strakovskaya, "Using pyroelectric detector for the dosimetry of pulsed ν-radiation", Instrum. Exp. Tech., Vol. 19, pp. 813-817, 1976.

[8] A. Rosencwaig and A. Gersho, "Theory of the photoacoustic effect with solids", J. Appl. Phys., Vol. 47, pp. 64-69, 1976.

[9] L.C. Aamodt and J.C. Murphy, "Size considerations in the design of cells for photoacoustic espectroscopy. II .Pulsed excitation response", J. Appl. Phys., Vol. 49, pp. 3036-3045, 1978.

[10] J. Cooper, "Minimum Detectable Power of a Pyroelectric Thermal Receiver", Rev. Sci. Instrum., Vol. 33, pp. 92-95, 1962.

List of Figure Captions

Fig. 1 - Schematic diagram of the photoacoustic radiation dosimeter.

Fig. 2 - Schematic drawing of the PERD and PPERD pyroelectric chamber, (1) cover, (2) Pyroelectric chamber casing, (3) Mylar window, (4) nylon support, (5) piezoelectric crystal, (6) orifice (to permite air exit), (7) BNC connector, (8) casing support, and (9) valve.

Fig. 3 - X-ray lead shutter, D: lead disk, O: orifice, M: motor, S: support.

Fig. 4 - Waveform of the electrical pulse produced by PPERD for $\Psi = 0.83\ J/m^2$, a = 0.32 s, b = 0.55 s, c = 0.74 s, d = 2.00 s, $V_I = -31.7$ mV, $V_S = 13.5$ mV.

Fig. 5 - Equivalent circuit of the pyroelectric detector and input amplifier. $R_1 = R_d//R_a$, $C_1 = C_d//C_a$ where R_d = equivalent detector resistance, R_a = preamplifier input resistance, C_a = capacitance of the amplifier, C_d = capacitance of the detector.

Fig. 6 - Diagram of the second stage of the preamplifier.

Fig. 7 - Cross section of the collimated x-ray beam.

Fig. 8 - Waveform of the power of the x-radiation pulse that strikes the pyroelectric detector. P_m is the maximum value of the power of the pulse.

Fig. 9 - Approximated waveform of the power of the x-radiation pulse.

Fig. 10 - Ilustration of $P(t) = \sum_{i=1}^{4} P_i(t)$.

Fig. 11 - Waveform of the electrical pulse produced by PPERD using the theoretical model, for $\Psi = 0.83\ J/m^2$. a = 0.16 s, b = 0.26 s, c = 0.36 s, d = 1.33 s, $V_I = -18.4$ mV, $V_S = 8.1$ mV.

Fig. 12 - (a) PARD voltage as a function of energy fluence rate.
(b) PERD voltage as a function of energy fluence rate.

Fig. 13 - (a) Response of the PPARD with the energy fluence.
(b) Response of the PPERD with the energy fluence.

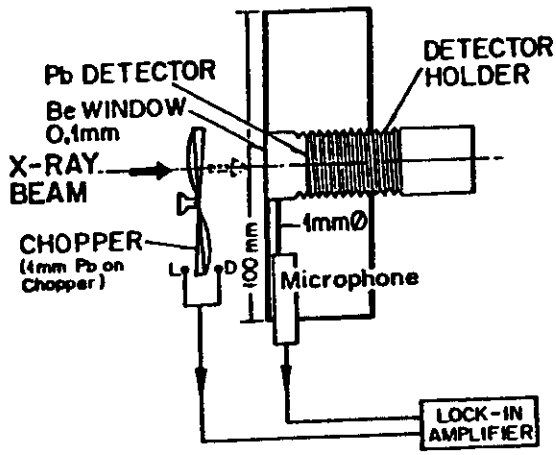
Pb DETECTOR
Be WINDOW
0,1mm
X-RAY
BEAM
CHOPPER
(1mm Pb on
Chopper)
D
100 mm
1mmØ
Microphone
DETECTOR
HOLDER
LOCK-IN
AMPLIFIER

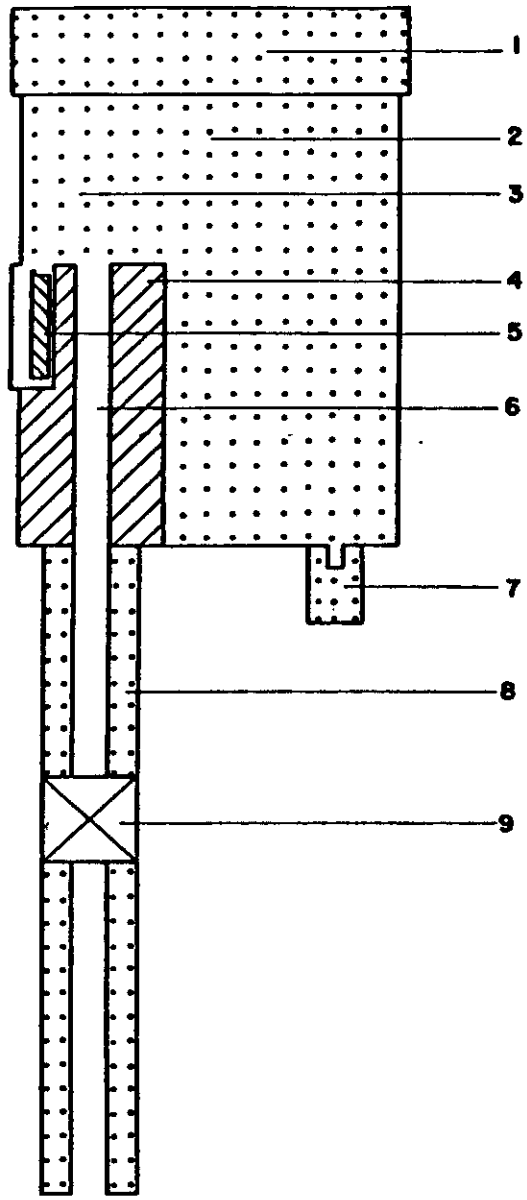

Fig 2

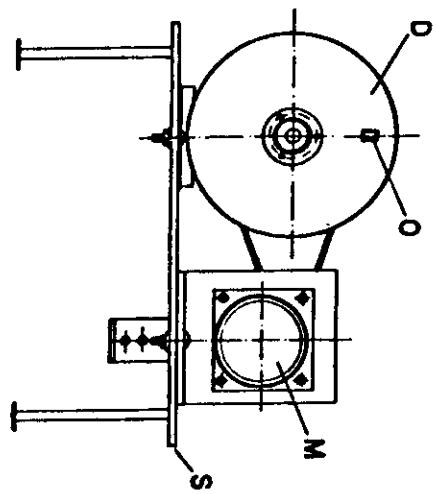
D
O
M
S

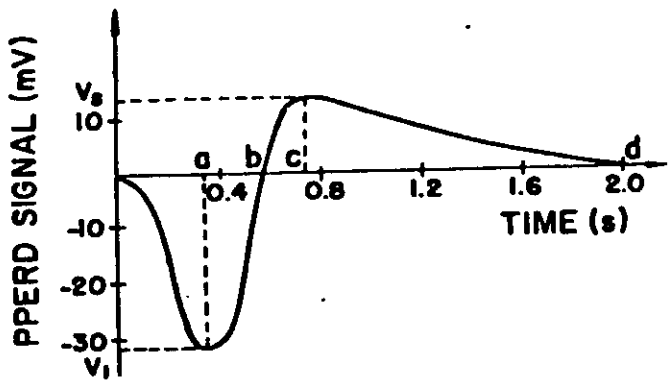
PPERD SIGNAL (mV)
V_s
10
-10
-20
-30
V_1
a
b
c
d
0.4
0.8
1.2
1.6
2.0
TIME (s)

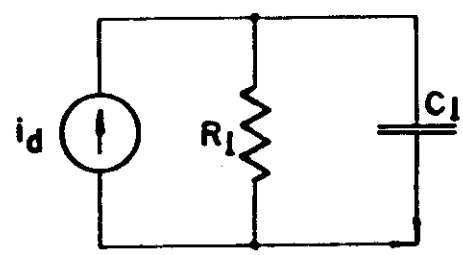
i_d
R_1
C_1

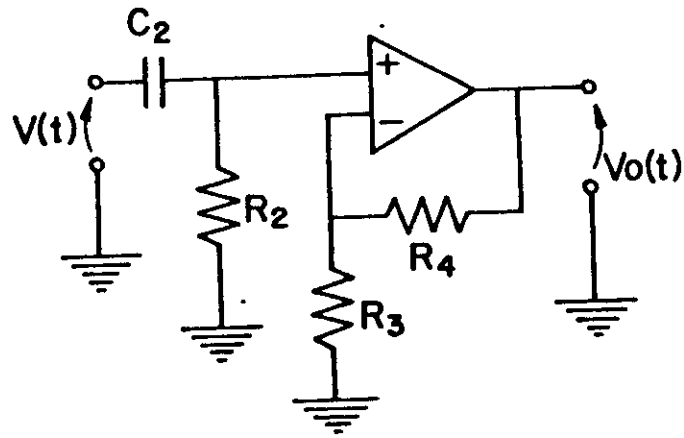
C2
V(t)
R2
R3
R4
Vo(t)
+
−

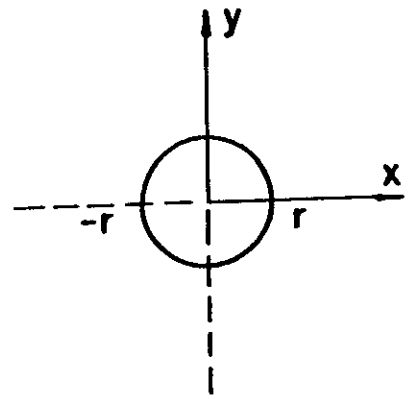
y
x
-r
r

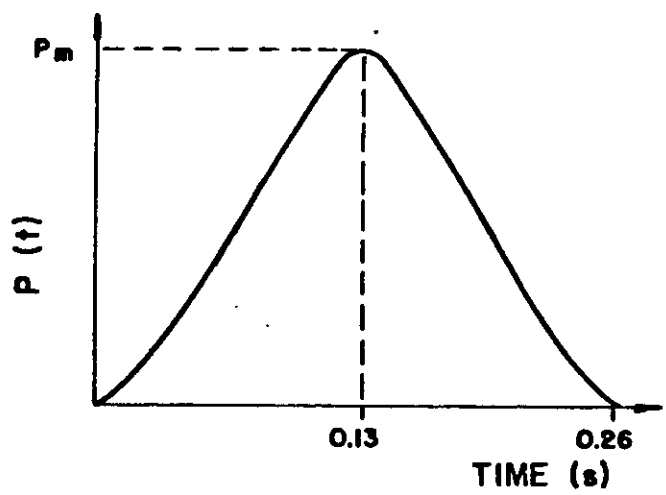
P_m
P (t)
0.13
0.26
TIME (s)

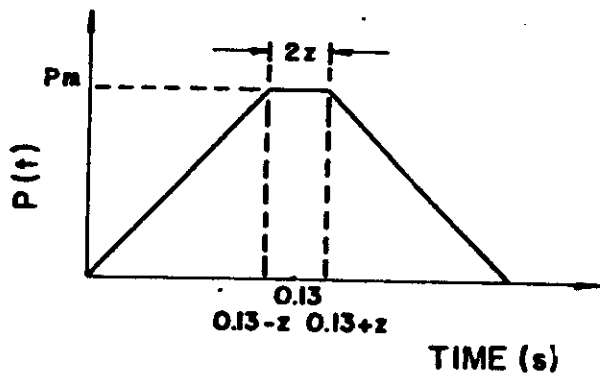
2z
Pm
P(t)
0.13
0.13-z 0.13+z
TIME (s)

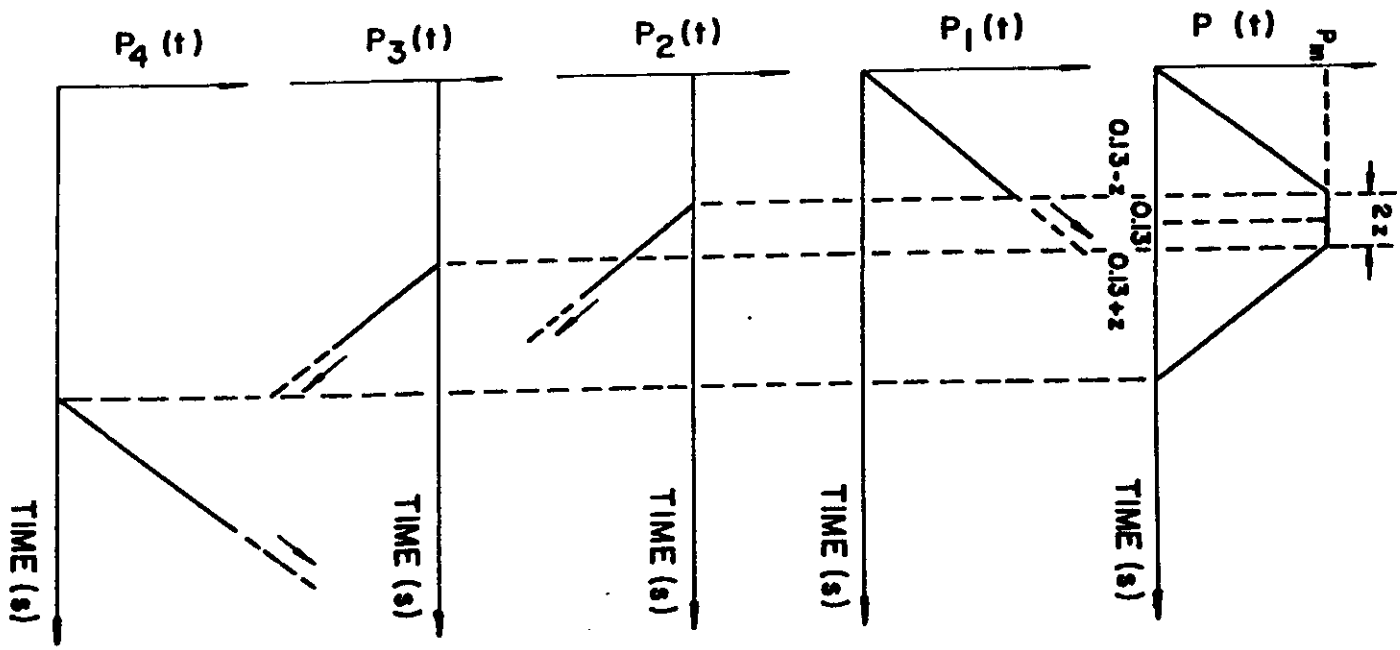
P4 (t)
P3(t)
P2(t)
P1(t)
P (t)
Pm
0.13-z
0.13
0.13+z
2z
TIME (s)
TIME (s)
TIME (s)
TIME (s)
TIME (s)

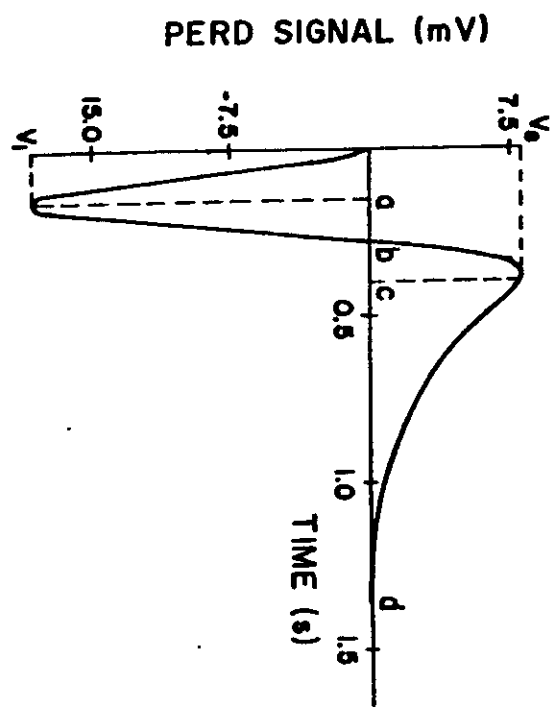
PERD SIGNAL (mV)
15.0
-7.5
7.5
V1
V2
a
b
c
d
0.5
1.0
1.5
TIME (s)

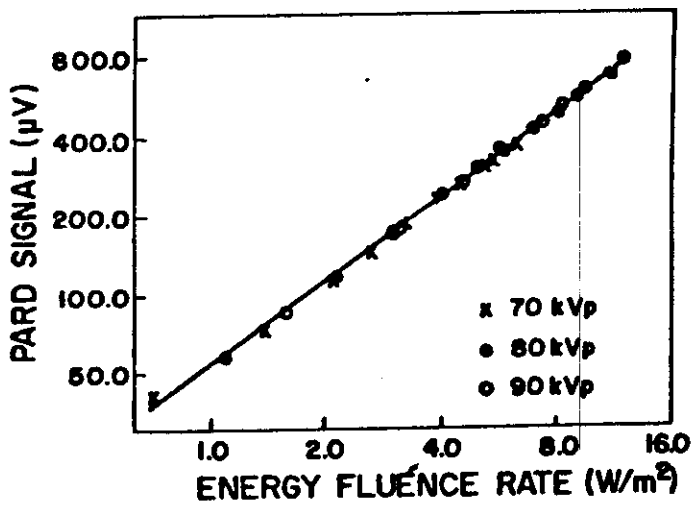
800.0
400.0
200.0
100.0
50.0
PARD SIGNAL (μV)
x 70 kVp
• 80 kVp
o 90 kVp
1.0
2.0
4.0
8.0
16.0
ENERGY FLUENCE RATE (W/m²)

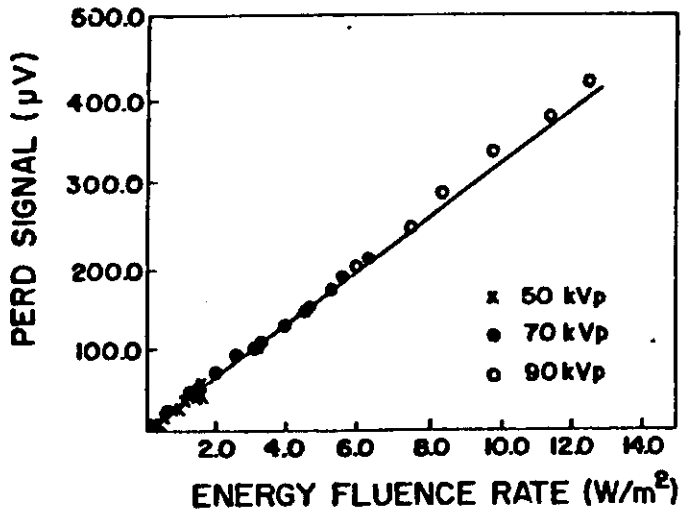
500.0
400.0
300.0
200.0
100.0
PERD SIGNAL (μV)
x 50 kVp
• 70 kVp
o 90 kVp
2.0
4.0
6.0
8.0
10.0
12.0
14.0
ENERGY FLUENCE RATE (W/m²)

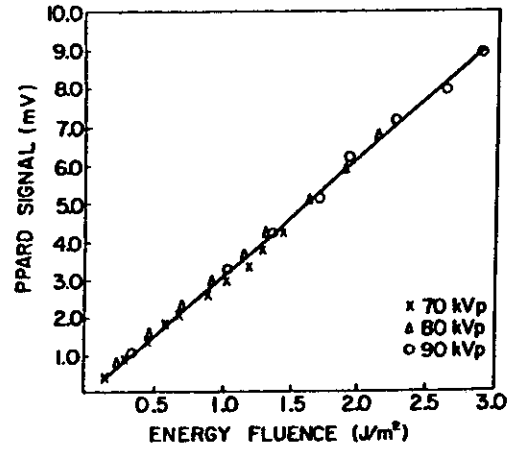
PPARD SIGNAL (mV)
10.0
9.0
8.0
7.0
6.0
5.0
4.0
3.0
2.0
1.0
0.5
1.0
1.5
2.0
2.5
3.0
ENERGY FLUENCE (J/m²)
x 70 kVp
▲ 80 kVp
o 90 kVp

Fig 13a

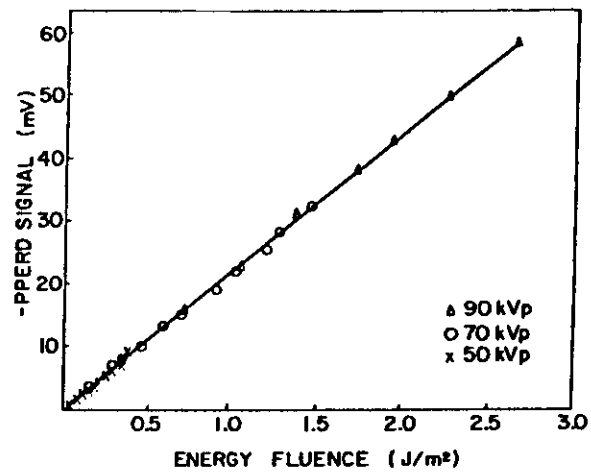
-PPERD SIGNAL (mV)
60
50
40
30
20
10
0.5
1.0
1.5
2.0
2.5
3.0
ENERGY FLUENCE (J/m²)
Δ 90 kVp
O 70 kVp
x 50 kVp